The effect of size on the quantitative estimation of defect depth in steel structures using lock-in thermography

C. Wallbrink,[a] S. A. Wade, and R. Jones
Department of Mechanical Engineering, Monash University, Victoria 3800, Australia and Commonwealth Research Centre for Integrated Engineering Asset Management (CIEAM), Monash University, Victoria 3800, Australia

(Received 5 November 2006; accepted 12 March 2007; published online 23 May 2007)

An investigation into the effect of size on the quantitative estimation of defect depth in a steel specimen has been undertaken using lock-in thermography. Phase contrast measurements over circular defects of varying diameter and depth are presented for a range of excitation frequencies. It was found that the diameter of a defect had an appreciable effect on the observed phase angle which consequently has significant implications with regard to estimating defect depth. Phase contrast measurements for a range of defects in a 10 mm steel specimen indicate that an excitation frequency of 0.02 Hz is the optimal frequency for defect detection. Results obtained with an excitation frequency of 0.02 Hz are used to discuss the limitations of determining the size and depth of defects. A finite element analysis was found to have good correlation with experimental data and thus demonstrates potential in providing improved estimates of defect depth. © *2007 American Institute of Physics*. [DOI: 10.1063/1.2732443]

I. INTRODUCTION

In the last decade, there has been a significant amount of interest into the use of infrared (IR) technology in areas of academic endeavour and industry. The main areas of research have investigated the use of IR technology as a tool in nondestructive evaluation (NDE) of structures such as bridges, buildings, and aircraft.[1–5] Thermographic techniques have shown several advantages over other forms of NDE. Perhaps the main advantage is its ability to examine wide areas simultaneously. Due to the diffusive nature of thermal signals in materials, there is a nonlinear drop in detectability of anomalies below the surface. Thus, IR technologies used for NDE are typically best suited to thin structures, such as those found in the aerospace industry. IR thermographic techniques have been used to examine aluminum structures with great success.[2,3,6] However, previous studies involving steel structures[7] have had limited success due in part to the requirement of large amounts of absorbed energy. The present research seeks to aid understanding of the limits of lock-in thermography for defect detection in steel structures and, in particular, the effect of defect size on the estimation of defect depth.

Most current thermographic methodologies employed to probe subsurface structures find their origins in photoacoustic research, where the structure under investigation gives an audible acoustic response as a result of an optically induced cyclic thermal excitation. Bell studied the use of optically induced acoustic waves in the 1880s, which resulted in several patents.[8] The effect in relation to solids was largely forgotten until Rosencwaig[9–11] was able to highlight several advantages compared to optical spectroscopy. Busse[12] extended the work of Rosencwaig, highlighting the significance of using the phase angle as a measure of depth. Busse[13] then published further results, demonstrating how the technique could be used to image changes in surface thermal properties and used as a method of subsurface imaging. Some of the earliest reviews on thermography were written in the mid-1980s and give a general overview of this emerging technology.[14,15]

In addition to monitoring the audible acoustic response, a number of other techniques to detect subsurface features were developed including the use of piezoceramic transducers[16–18] (PZTs) and the beam deflection technique.[18–20] A major advance in detection techniques occurred with the development of photothermal detectors to detect the infrared radiation emitted from the excited material. Busse[21] was able to apply this technology to probe metallic structures of varying thicknesses. The significance of this technique as a nondestructive tool was quickly embraced, producing a significant amount of research.[22–25]

A significant improvement in radiation infrared detection came about with the advent of focal plane arrays. Focal plane arrays are made from small elements of photosensitive media that are generally aligned in a square matrix configuration. Similar to the photosensitive diode in digital cameras, each element represents a pixel in the picture. The more densely packed the array is, the higher the resolution of the picture. Busse *et al.*[26] suggested the use of a focal plane IR detector together with remote lamps in a thermographic technique known as the modulated or optical lock-in thermography.

Lock-in thermography and the related pulse phase thermography method typically use phase angle measurements for the assessment of underlying defects.[1,27] In the case of lock-in thermography, the phase angle refers to the phase difference $\Delta\phi$ between a sinusoidally modulated incident thermal flux and the associated thermal response, as illustrated in Fig. 1. In pulse phase thermography, the phase angle is determined indirectly, typically by perfoming a Fourier

[a]Electronic mail: chris.wallbrink@dsto.defence.gov.au

 © 2007 American Institute of Physics

Downloaded 02 Aug 2011 to 136.186.80.71. Redistribution subject to AIP license or copyright; see http://jap.aip.org/about/rights_and_permissions

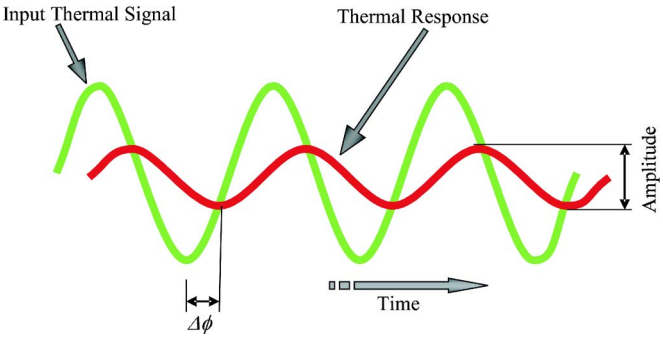

FIG. 1. A sinusoidal thermal input signal and the associated thermal response.

transform on a recorded thermal time history. One of the advantages of using the phase angle measurement is a greater depth penetration, often quoted[28,29] as $p=1.8\mu$, as compared to amplitude data, where p is the penetration depth and μ is the thermal diffusion length. However, while phase angle images can easily be obtained, difficulties remain with obtaining quantitative measurements from the recorded images.

Recently, work has been undertaken to understand the geometrical limitations of defect detection with lock-in thermography. Meola *et al.*[30] have investigated the effects of defect size, depth, and thickness in composite panels using lock-in thermography. In this work, it was found that thin defects in composites were harder to detect than thicker defects. Other work by Maldague[31] mentions an empirical rule of thumb that for a homogeneous isotropic material the smallest detectable defect should be no deeper than its diameter. Ongoing work using pulse phase thermographic techniques is being conducted to understand the observed changes in phase angle at the edges of defects. Almond and Lau[32,33] have shown that the decay of thermal response occurs over approximately one diffusion length over the edge of a defect; however, their analysis is strictly valid for infinitely thin defects that have a diameter larger than one diffusion length. Saintey and Almond[34] showed a divergence between current analytical models and their finite difference model which they attributed to simplifying assumptions in the analytical models. Krapez *et al.*[35,36] have developed a numerical inversion technique to extract depth and size information, while Maldague *et al.*[37] have used a neural network to extract quantitative information.

One approach to determining quantitative information about the depth of a defect is to use a relationship based on a one-dimensional approximation.[38–40] However, in real world structures this approximation can be an oversimplification as three-dimensional heat flow effects will tend to dominate. Lock-in thermography has a great potential as a nondestructive inspection (NDI) tool but requires a good understanding of the limitations with respect to the detectable depth and size of defects. In this study, we investigate the limitations of the lock-in thermographic technique and provide guidance to estimate defect severity by examining a steel specimen with cutouts of various sizes. In addition, the results of a preliminary finite element study will be used to support the conclusions herein.

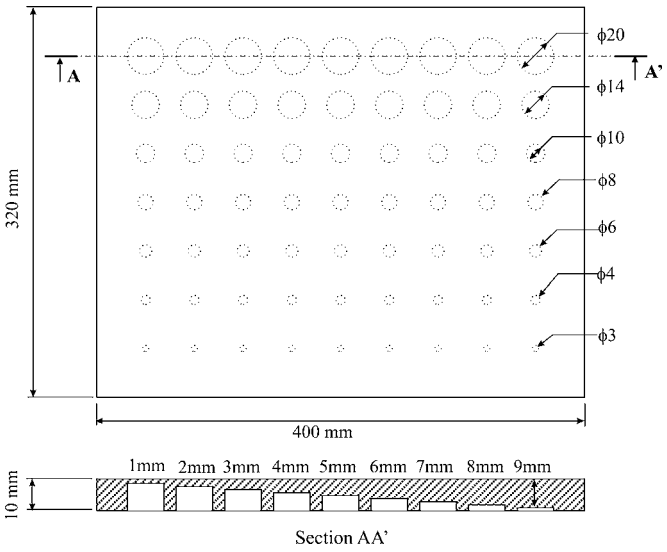

FIG. 2. 10 mm thick steel specimen (not to scale).

II. METHOD

In the present investigation, a sinusoidal thermal source was used to excite the surface of a steel specimen with cutouts on the opposite side. The response of the thermally excited surface was recorded simultaneously using an infrared camera. Real time analysis of both signals was performed to determine the associated phase angle using a commercially available lock-in box.

A mild steel plate specimen 10 mm thick with circular cutouts of varying depth and diameter was manufactured. The idealized shape of a circular defect was chosen in this investigation to illustrate the effects of geometry on the observed thermal response. Figure 2 shows the geometry of the test specimen used in the present investigation. The 20 mm diameter, 1 mm deep defect is located in the top left hand corner, i.e., a 9 mm deep circular blind hole was milled into the plate to produce a defect 1 mm beneath the sound surface. In this study, the defect depth refers to the remnant thickness of material between the base of the circular cutout and the sound surface of the specimen. Each row of cutouts in the steel plate in Fig. 2 represents defects of constant diameter but at increasing depth moving left to right. Each vertical column of cutouts represents defects of constant depth but decreasing diameter moving top to bottom.

A schematic of the general test arrangement is presented in Fig. 3. The lock-in thermographic system used six 750 W Source-Four lamps to provide the thermal excitation. To prevent direct reflection back into the camera, the lamps were oriented on either side of the specimen. A Hameg HM8131-2 function generator was used to sinusoidally modulate the intensity of the lamps.

The acquisition system consisted of a laptop computer connected to the infrared camera and a commercially available external hardware device known as the lock-in box. The infrared system used was a Cedip Jade 3 midwavelength infrared (MWIR) camera, which operates in the midwavelength infrared spectral range (3.7–4.8 μm). This system uses a $Hg_xCd_{1-x}Te$ (MCT) detector array producing images with a resolution of 320×240 pixels and has a quoted ther-

Downloaded 02 Aug 2011 to 136.186.80.71. Redistribution subject to AIP license or copyright; see http://jap.aip.org/about/rights_and_permissions

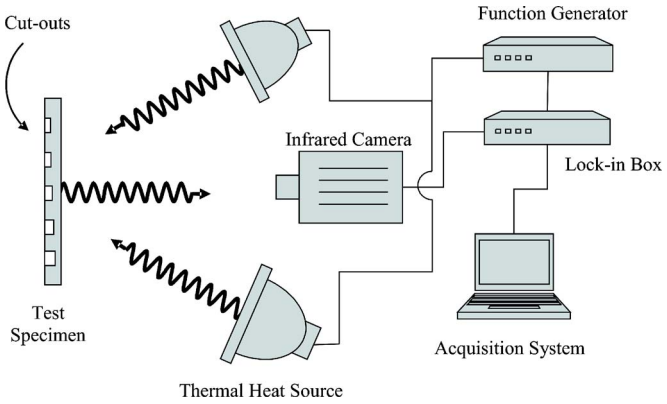

FIG. 3. A schematic of the experimental arrangement used to perform optical lock-in measurements.

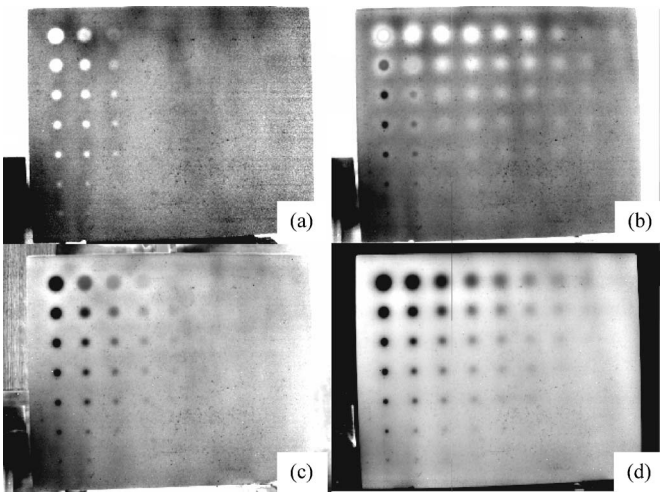

FIG. 4. Thermal phase angle images recorded using and thermal excitation frequencies of (a) 0.8 Hz, (b) 0.1 Hz, (c) 0.05 Hz, and (d) 0.02 Hz.

mal sensitivity of less than 25 mK for temperatures above 25 °C. A 50 mm lens was used in the current investigation with the camera positioned to fully utilize the field of view encompassing the entire specimen. The lock-in box is a hardware device supplied by Cedip Infrared Systems that compares an input signal to the time history of every pixel in the focal plane array, allowing phase angle and amplitude information to be obtained. The exact mode of operation remains proprietary information.

The test sample was positioned vertically with the sound side of the plate (i.e., the side without cutouts) exposed to the excitation source. The sound side of the plate was painted with RS 496-782 Matt Black paint which has an emissivity of approximately 0.92.[41] The specimen was painted black to increase the surface emissivity of the specimen and provide a uniformly emissive surface.

A range of modulation frequencies was used to interrogate the steel sample ranging from 0.8 down to 0.005 Hz. The camera frame rate was set to 50 frames/s with acquisition times for each frequency roughly kept equal. Longer acquisition times were required for the low frequencies to obtain a number of periods with which to average. A higher degree of noise was observed at high frequencies (in the present discussion, high frequencies refer to frequencies around 0.8 Hz). Increasing the number of periods aided in reducing the noise level and to improve image clarity.

III. RESULTS

In the following sections, examples of some of the lock-in phase angle images obtained in this investigation are presented. Analysis of the recorded images is performed in relation to both defect depth and defect diameter, and an estimate of the absolute minimum detectable defects is presented. Finally, a preliminary finite element analysis is conducted and compared with a one-dimensional solution and the experimentally measured phase angle over the 20 mm diameter, 1 mm deep defect.

A. Phase angle images

Phase angle images were acquired for excitation frequencies between 0.8 and 0.005 Hz. Figure 4 shows examples of the thermal phase angle images acquired using thermal excitation frequencies of 0.8, 0.1, 0.05, and 0.02 Hz. The gray scale of each of the images has been adjusted to maximize the contrast between the defects and the sound material. The steel specimen in the images in Fig. 4 is oriented as in Fig. 2.

In Fig. 4(a), recorded with an excitation frequency of 0.8 Hz, defects are observed in the first three columns. As the frequency is decreased to 0.1 Hz, more columns become visible, as shown in Fig. 4(b). Noticeable in Fig. 4(b) is a phase contrast inversion taking place in the first two columns. Here, the defects which were initially observed as white dots are now black. The phase contrast refers to the phase difference between the phase angle measured over a defect and the phase angle in the sound material. In Fig. 4(c), almost full phase inversion has taken place; however, defects to the right of the plate are less visible than they appeared in Fig. 4(b). Several of the defects at this frequency are not visible to the right of the plate as the phase contrast is close to zero. Frequencies at which the phase contrast becomes zero are known as "blind frequencies." The majority of the defects were visible in Fig. 4(d), which was recorded with an excitation frequency of 0.02 Hz. As will be shown in Sec. III B, an excitation frequency of 0.02 Hz provided the best phase angle response. In general, in Fig. 4, we also observed that the edges of the defect become increasingly more diffuse as the defects become deeper (i.e., remnant thickness of material increases).

B. Analysis of the effect of depth on phase contrast

Using the thermal phase angle images recorded, the phase contrast was evaluated by subtracting the phase angle located centrally over the defects from the phase angle measured in the sound material located near the circular cutouts. The phase contrast was then plotted for each of the defects as a function of excitation frequency. Figure 5 shows the phase contrast evaluated for the defects with a 20 mm diameter at various depths from the sound surface. Results for the defect with a 20 mm diameter at a depth of 9 mm have not been plotted, as the thermal response fell below the ambient noise

Downloaded 02 Aug 2011 to 136.186.80.71. Redistribution subject to AIP license or copyright; see http://jap.aip.org/about/rights_and_permissions

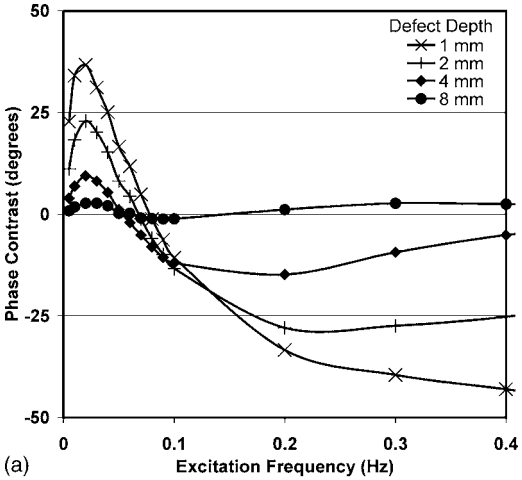

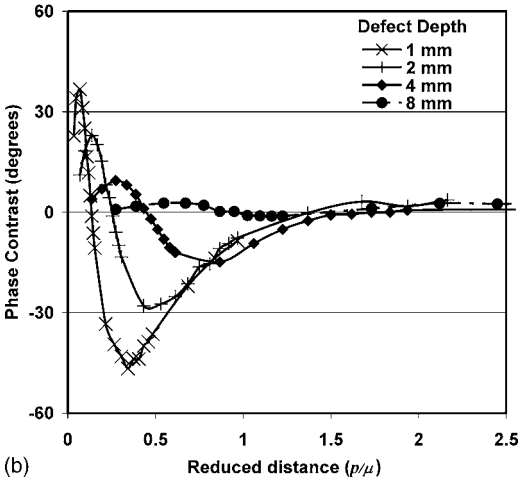

FIG. 5. Phase contrast for the 20 mm diameter blind holes (a) as a function of the thermal excitation frequency and (b) as a function of the reduced distance.

level of the infrared detector array. Errors were evaluated by examining the two standard deviations associated with pixel noise in the sound material. Errors have not been presented in the figures as they are of the same order of magnitude as the symbols used to plot the data. Although data were obtained to 0.8 Hz, the following figures contain data up to 0.4 Hz to accentuate low modulation frequency effects.

Figure 5(a) can be used to select an appropriate frequency to provide the largest thermal contrast for NDE purposes. In the present study, a frequency of 0.02 Hz provides good contrast for defects at all the depths of interest. An inversion of the phase contrast (i.e., when the two signals are in phase with each other) occurs in a frequency range of 0.05–0.08 Hz. At higher frequencies, good thermal contrasts are achieved at ~0.2 Hz and then the magnitude of the contrasts tapers off as the thermal excitation frequency is increased. Although good thermal contrast is achieved for shallow defects (i.e., small remnant thicknesses) at these frequencies, deeper defects are not easily detected. The data in Fig. 5(a) have been replotted in terms of the reduced distance in Fig. 5(b). The reduced distance is defined as the depth of the defect divided by the thermal diffusion length.

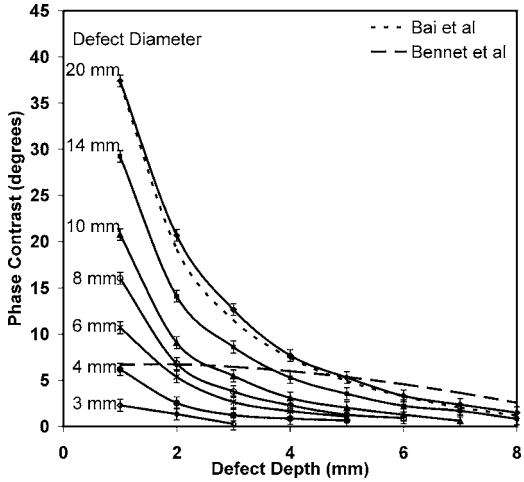

FIG. 6. The phase contrast for various defect diameters as a function of section thickness obtained with a thermal excitation frequency of 0.02 Hz, together with theoretical solutions for comparison.

The present investigation has shown [Fig. 5(b)] that the large diameter defects are first detected at approximately 1.6μ, consistent with earlier observations.[13]

Figure 6 shows the phase contrast measured over the defects as a function of defect depth for a thermal excitation frequency of 0.02 Hz. As can be seen in Fig. 6, the rate at which the phase contrast is affected by defect depth decreases in an almost exponential manner. Also plotted in Fig. 6 are the one-dimensional solutions proposed by Bai and Wong[38] and that of Bennet and Patty.[40] A further discussion comparing the one-dimensional solution to the present experimental results will be presented later in the text.

C. Analysis of the effect of defect diameter on phase contrast

The phase contrast for defects with differing diameter at a constant depth of 1 mm from the sound surface has been plotted in Fig. 7 along with the one-dimensional solutions proposed by Bai and Wong[38] and that of Bennet and Patty.[40] Here, the thermal phase angle displays a significantly differ-

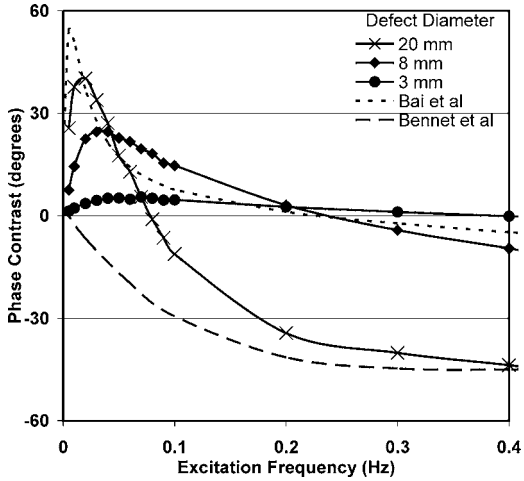

FIG. 7. Comparison of thermal phase contrast curves for defects of varying diameter at a constant depth of 1 mm from the sound surface, together with theoretical solutions for comparison.

Downloaded 02 Aug 2011 to 136.186.80.71. Redistribution subject to AIP license or copyright; see http://jap.aip.org/about/rights_and_permissions

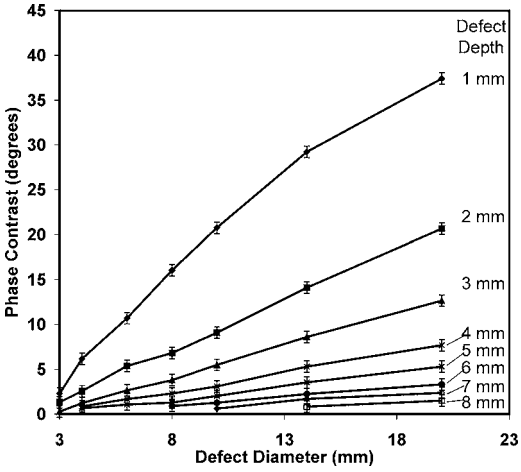

FIG. 8. A comparison of phase contrast for defects of increasing depth as a function of defect diameter recorded using a thermal excitation frequency of 0.02 Hz.

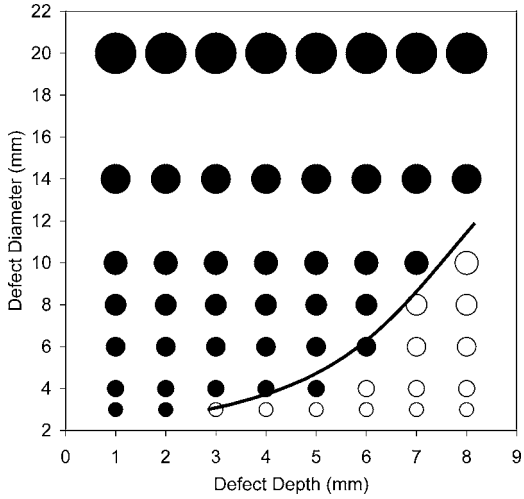

FIG. 9. The smallest detectable defect as a function of depth for the steel plate tested with a thermal excitation frequency of 0.02 Hz. Black circles indicate defects that were detected and white circles indicate defects not detected using Eq. (1).

ent response to frequency as the defect diameter changes compared with the defect depth data shown in Fig. 5.

In comparison with Fig. 5, the blind frequencies in Fig. 7 show a significant dependence on the defect diameter, indicating that defect size will have an appreciable effect on the phase angle measurement. Also plotted in Fig. 7 are the solutions proposed by Bai and Wong[38] and that of Bennet and Patty[40] based on a one-dimensional approximation which gives the same result regardless of the defect diameter and clearly differs from the observed data. The dependence of the phase contrast on the excitation frequency indicates that lateral diffusion of heat energy has an appreciable effect, which has significant implications when estimating the associate defect depth.

Figure 8 shows a comparison of the maximum phase angle contrast measured over each defect as a function of defect diameter. The one-dimensional approximations previously discussed give a constant phase contrast for different diameters which is clearly different from the data shown in Fig. 8. The effect is more pronounced for smaller diameter defects, indicating that a larger component of thermal energy diffuses laterally in the material.

D. Limits of defect detection using lock-in thermography

The present phase angle measurements have an associated level of background noise that will interfere with the detection of defects. The noise in the image results from several sources but primarily from the sensitivity of individual pixels in the focal plane array of the camera. The ability to detect a defect requires that the phase change caused by the defect is greater than the background noise. This has been investigated for the test arrangement used in this work for the excitation frequency of 0.02 Hz which was earlier found to give good phase contrast for the majority of the plate defects. The sound areas of the steel specimen in Fig. 4(d) contain a standard deviation (σ_s) of approximately 0.17° for the excitation frequency of 0.02 Hz. We can use this value to estimate the limit of detectability for the excitation frequency of 0.02 Hz. If we assume that phase angle measurements over the defects contain the same level of noise (σ_d), then we can set a limit below which detection of defects becomes hidden by the noise in the phase angle measurements. Equation (1) sets a limit criterion on the detectability of defects associated with phase contrast measurements, where D_L represents the limiting phase. Two standard deviations were used to represent 95% confidence intervals for measurements of phase in the sound material and over the defects.

$$D_L = 2\sigma_S + 2\sigma_d. \tag{1}$$

When the local phase contrast over a defect is greater that D_L, then a defect is detected and below D_L a defect is not detected.

The curve in Fig. 9 represents the minimum detectable defect as a function of depth using D_L as the smallest detectable phase contrast. Defects that lie to the left of the curve are detectable via the present technique and those to the right of the curve fall below the limit set in Eq. (1) and are difficult to detect. In Fig. 9, black circles indicate defects experimentally detected with phase contrasts above D_L, while white circles indicate defects with phase contrasts below D_L. To determine the limiting curve in Fig. 9, a three-dimensional surface fit was performed. A least squares polynomial fit was used in conjunction with the limiting phase contrast D_L to determine the limiting relationship between the defect diameter and the depth of the defect. It is important to note that the curve plotted in Fig. 9 is associated with an excitation frequency of 0.02 Hz which was experimentally determined to give the best phase contrast (refer to Sec. III B). This curve will change depending on the excitation frequency, and hence the number and size of the defects detected via this method will also change.

Downloaded 02 Aug 2011 to 136.186.80.71. Redistribution subject to AIP license or copyright; see http://jap.aip.org/about/rights_and_permissions

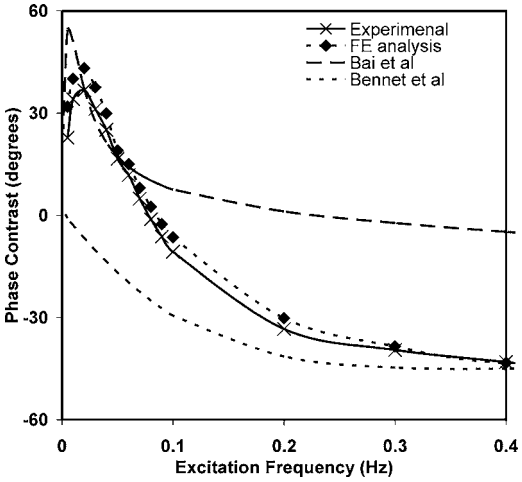

FIG. 10. A comparison of the experimentally measured phase contrast and the results from a finite element analysis and one-dimensional solutions for a defect 20 mm in diameter at a depth of 1 mm in a 10 mm thick steel plate.

E. Finite element analysis considering three-dimensional heat flow effects

A finite element (FE) study was conducted to establish the validity of the phase contrast measurements and examine the effect of lateral heat diffusion on the lock-in thermography technique. A finite element analysis was performed for a defect 20 mm in diameter and 1 mm below the surface of a 10 mm thick steel plate. Experimentally, this defect provided the largest phase response and thus the largest signal to noise ratio. The following properties were used for the mild steel plate: a density of 7858 kg/m^3, a thermal conductivity of 51.2 W/m K, and a specific heat of 486 J/kg K. The finite element analysis was conducted using NE/Nastran in the transient heat transfer mode. The defect was modeled as a round cutout centrally located in a flat disk. In this configuration, no lateral diffusion of heat should take place tangentially to the radial direction. Taking advantage of symmetry, a two-dimensional slice was used to model the thermal response to a sinusoidally modulated heat flux. The temperature time history was monitored directly over the defect and also in the sound material. The temperature time histories at these locations were then used to determine the phase contrast associated with the frequency of the sinusoidal wave form. The results have been plotted in Fig. 10 and are compared with the experimental data. Good correlation is achieved between the experimental observation and the finite element analysis. Also shown for comparison in Fig. 10 are the one-dimensional solutions by Bai and Wong[38] and that of Bennet and Patty.[40] The maximum experimentally measured phase contrast at 0.02 Hz is slightly lower than that predicted by the finite element analysis; however, this is expected as the experimental measurements of the phase angle were obtained over a small area located on the defect rather than a point measurement. The pixel resolution of the camera therefore effectively averages the result over the area to which the pixel represents.

IV. DISCUSSION

For the purpose of nondestructive evaluation, it is important to understand the limitations of the lock-in thermographic system in order to make accurate engineering judgments about the condition of a structure. The results of the current investigation have shown that the measured phase angle recorded using lock-in thermography is affected not only by its depth but also by its diameter. An excitation frequency of 0.02 Hz was experimentally determined to provide the strongest phase contrast response for defects in the 10 mm steel plate investigated. Using this excitation frequency, an estimate of the smallest defect as a function of depth was obtained. Maldague[31] suggested that an empirical rule of thumb was that the smallest detectable defect should be no deeper than its diameter. Referring to Fig. 9, it would appear that this rule of thumb holds, but for defects no deeper than 5 mm from the sound surface in a steel structure. The results in Fig. 9 indicate that defects become increasingly more difficult to detect for defects of increasing depth in an almost exponential manner.

In this work, the phase contrast was observed to decay exponentially as the depth of the defect increased (see Fig. 6); thus, deeper defects are much harder to resolve. The ability to detect defects is also a function of the excitation frequency and the signal to noise ratio of the thermographic equipment. Thus, improvements in the signal to noise ratio of the detector should lead to enhancements in defect detection. This can be achieved with further improvements in sensitivity and resolution of infrared detector arrays. Introducing larger amounts of energy to the structure could also aid in resolving defects by increasing the signal to noise ratio but may not be a practical alternative. Another method typically used to reduce noise is to average the signal. In the present investigation, the time history recorded for the specimen at each frequency involved approximately 5000 images. However, it was observed that any further increase in the number of images acquired resulted in an insignificant reduction in the level of noise.

Almond and Lau[32,33] have shown that for a cracklike defect, the temperature decays over a distance of approximately one diffusion length from the edge of the defect. Certainly, the present observations seem to support this conclusion. Bennet and Patty[40] have developed a one-dimensional solution considering conductive effects ignoring convective and radiative effects. As seen in Fig. 10, their solution compares well for the 20 mm diameter defect for high frequencies but diverges for lower modulation frequencies. The divergence of the solution could possibly be attributed to increased influences of convective and radiative effects at lower frequencies and lateral diffusion in the structure. The solution by Bai and Wong,[38] which considers convection and radiation, does not compare well for high modulation frequencies but appears to have the correct functional form for low modulation frequencies. The close agreement at low modulation frequencies suggests that convective and radiative effects were beginning to have a greater influence. For the majority of the defects considered in this investigation, the diffusion length exceeded the diameter of the defect and thus edge effects begin to dominate the response as suggested by Almond and Lau.[32,33]

The presence of scattered surface defects and foreign material on the surface of the specimen introduced spurious

Downloaded 02 Aug 2011 to 136.186.80.71. Redistribution subject to AIP license or copyright; see http://jap.aip.org/about/rights_and_permissions

changes in the observed phase angle. These changes in phase angle could be construed as a subsurface defect without prior knowledge of the surface condition. It was found, however, that the effect of surface irregularities appears to diminish with decreasing excitation frequency. The low frequencies while providing the strongest phase contrast response also provided the most insensitive response to surface irregularities. One explanation is that these surface irregularities have a lower thermal conductivity and thus affected phase more readily at higher frequencies.

A comparison was made in Figs. 6 and 7 between the phase contrast calculated using a one-dimensional approximation[38] and the experimentally measured phase contrast. As the diameter of the defect decreases, lateral heat flow effects increasingly dominate the observed phase contrast, resulting in differences between the one-dimensional approximation and the experimentally observed results. Figure 6 shows the phase contrast plotted as a function of defect depth in comparison with the one-dimensional approximation. The solution of Bai and Wong[38] is in good agreement with results obtained for the 20 mm diameter defect; however, this is more likely to be coincidental and associated with the chosen frequency of 0.02 Hz. The solution of Bennet and Patty[40] does not agree with the observed results at this frequency, as previously discussed. Notably all the other defects display decreasing phase angle measurements as the diameter decreases. Hence, if a technician was to measure the phase angle over a defect 6 mm in diameter and use the one-dimensional approximation proposed by Bai and Wong[38] to estimate the defect depth, they could mistakenly interpret the result as a defect 3.5 mm below the surface, when, in fact, the defect is only 1 mm below the surface. As such, if the defect diameter varies, the use of a one-dimensional approximation to estimate the depth of a defect based on the phase angle could lead to erroneous measurements of depth. Indeed, Fig. 10 shows that modeling lateral heat flow with techniques such as finite element analysis provides a much better means of estimating defect depth.

For real world NDI problems, the underlying changes in material structure are unknown and are rarely uniform in nature, nor are they circular. As we do not know the true underlying changes in geometry, it becomes difficult to estimate the extent of thickness variation due to three-dimensional heat flow effects. To properly understand and make predictions with regard to the size and thickness of defects, a more sophisticated approach is required. Here, preliminary finite element analysis has been used to model the three-dimensional heat flow dynamics and has shown excellent agreement with experimentally obtained results. This would suggest that a finite element analysis is one available method that could be used to more accurately characterize hidden internal changes in geometry and material in real world applications.

V. CONCLUSION

An investigation into the effect of size on the quantitative estimation of defect depth was undertaken using lock-in thermography using a 10 mm thick steel specimen containing circular defects of varying size and depth. Phase angle measurements were obtained for a range of thermal excitation frequencies for each of the defects in the steel specimen. An excitation frequency of 0.02 Hz was found to provide phase angle images with the best thermal contrast for the range of defects considered in this study. The limits of defect detectability were examined using phase angle measurements obtained using the optimal excitation frequency of 0.02 Hz.

The present investigation found that both defect diameter and defect depth (i.e., remnant material thickness) had appreciable effects on the observed phase angle. The observed changes in phase angle have been attributed to lateral diffusion of heat in the steel specimen. An investigation into the smallest detectable defects was conducted and a relationship between defect diameter and defect depth was found. For a defect at a depth of 3 mm from the sound surface, the smallest defect diameter that could be detected was estimated to be 3 mm. As the defect depth increased (i.e., the remnant material thickness increased), there appeared to be an exponential increase in the smallest defect diameter which could be detected. For a defect at a depth of 8 mm, the smallest diameter defect that could be detected was estimated to be 11.5 mm. The detectability of defects was found to be associated with noise in the phase angle images. Thus, improvements in infrared detection to reduce the level of noise such as increases in sensitivity should lead to improvements in detectability.

A comparison with experimental data has shown that one-dimensional approximations such as that by Bai and Wong[38] and that of Bennet and Patty[40] are more appropriate to large diameter defects larger than the thermal diffusion length. In the case of Bennet and Patty,[40] the solution is valid in situations where conductive influences dominate and in the case of Bai and Wong[38] where convective and radiative influences dominate. The present investigation has shown application of these solutions to small defects may lead to erroneous conclusions about the depth of a defect. In contrast, preliminary finite element analysis has shown good correlation with the experimental measurements over a broad range of excitation frequencies. We suggest that a method such as finite element analysis, which considers multidimensional heat flow phenomenon, will provide more accurate estimates of defect depth.

ACKNOWLEDGMENTS

This work was conducted as part of the Commonwealth Research Centre for Integrated Engineering Asset Management (CIEAM). The authors gratefully acknowledge the support and assistance of Dr. Dian Arifin with the preparation of the manuscript.

[1]D. Wu, G. Zenzinger, W. Karpen, and G. Busse, Mater. Sci. Forum **210–213**, 289 (1996).
[2]D. Wu *et al.*, *Inspection of Aircraft Structural Components Using Lockin-Thermography* (Edizione ETS, Pisa, 1997), pp. 251–256.
[3]N. P. Avdelidis and D. P. Almond, NDT & E Int. **37**, 353 (2004).
[4]T. Zweschper, A. Dillenz, G. Riegert, and G. Busse, Proceedings of the 8th European Conference on Nondestructive Testing, Barcelona, 2002.

Downloaded 02 Aug 2011 to 136.186.80.71. Redistribution subject to AIP license or copyright; see http://jap.aip.org/about/rights_and_permissions

[5]N. K. Del Grande, Proceedings of the American Society for Nondestructive Testing, Long Beach, CA, 1993.
[6]N. Rajic, Res. Nondestruct. Eval. **12**, 119 (2000).
[7]V. P. Vavilov, Revista de Metalurgia (Madrid), 235 (2003).
[8]A. G. Bell, Am. J. Sci. **20**, 305 (1880).
[9]A. Rosencwaig, Opt. Commun. **7**, 305 (1973).
[10]A. Rosencwaig and A. Gersho, J. Appl. Phys. **47**, 64 (1976).
[11]A. Rosencwaig, J. Appl. Phys. **49**, 2905 (1978).
[12]G. Busse, Appl. Phys. Lett. **35**, 759 (1979).
[13]G. Busse, Opt. Laser Technol. **12**, 149 (1980).
[14]F. A. McDonald, Can. J. Phys. **64**, 1023 (1985).
[15]R. L. Thomas, L. D. Favro, and P. K. Kuo, Can. J. Phys. **64**, 1234 (1985).
[16]A. Hordvik and H. Schlossberg, Appl. Opt. **16**, 101 (1977).
[17]T. Nguyen and A. Rosencwaig, Appl. Surf. Sci. **24**, 57 (1985).
[18]A. Rosencwaig, J. Photoacoust. **1**, 371 (1982).
[19]L. C. Aamodt and J. C. Murphy, J. Appl. Phys. **52**, 4903 (1981).
[20]J. C. Murphy and L. C. Aamodt, Appl. Phys. Lett. **39**, 519 (1981).
[21]G. Busse, Infrared Phys. **20**, 419 (1980).
[22]M. Luukkala, A. Lehto, J. Jaarinen, and M. Jokinen, *Ultrasonics Symposium Proceedings*, San Diego, CA (IEEE, New York, 1982), pp. 591–594.
[23]D. P. Almond, P. M. Patel, I. M. Pickup, and H. Reiter, NDT Int. **18**, 17 (1985).
[24]D. P. Almond, P. M. Patel, J. D. Morris, and H. Reiter, Proceedings of the SPIE-The International Society for Optical Engineering, London, 1988, pp. 84–90.
[25]R. M. Miller, Proceedings of the SPIE-The International Society for Optical Engineering, San Diego, CA, 1986, pp. 16–22.
[26]G. Busse, D. Wu, and W. Karpen, J. Appl. Phys. **71**, 3962 (1992).
[27]C. Meola, G. M. Carlomagno, A. Squillace, and G. Giorleo, Meas. Sci. Technol. **13**, 1583 (2002).
[28]A. Rosencwaig and G. Busse, Appl. Phys. Lett. **36**, 725 (1980).
[29]C. Meola and G. M. Carlomagno, Meas. Sci. Technol. **15**, 27 (2004).
[30]C. Meola, G. M. Carlomagno, and L. Giorleo, J. Nondestruct. Eval. **23**, 125 (2004).
[31]X. Maldague, Mater. Eval. **60**, 1060 (2002).
[32]D. P. Almond and S. K. Lau, Appl. Phys. Lett. **62**, 3369 (1993).
[33]D. P. Almond and S. K. Lau, J. Phys. D **27**, 1063 (1994).
[34]M. B. Saintey and D. P. Almond, J. Phys. D **28**, 2539 (1995).
[35]J. C. Krapez and P. Cielo, Res. Nondestruct. Eval. **3**, 81 (1991).
[36]J. C. Krapez, X. Maldague, and P. Cielo, Res. Nondestruct. Eval. **3**, 101 (1991).
[37]X. Maldague, Y. Largouet, and J.-P. Couturier, Rev. Gen. Therm. **37**, 704 (1998).
[38]W. Bai and B. S. Wong, J. Appl. Phys. **89**, 3275 (2001).
[39]W. Bai and B. S. Wong, Meas. Sci. Technol. **12**, 142 (2001).
[40]C. A. Bennet and R. R. Patty, Appl. Opt. **21**, 49 (1982).
[41]Ometron Spate 8000 Manual.

Downloaded 02 Aug 2011 to 136.186.80.71. Redistribution subject to AIP license or copyright; see http://jap.aip.org/about/rights_and_permissions